



# Quantifying relative within-host replication fitness in influenza virus competition experiments



Stephen M. Petrie<sup>a,b</sup>, Jeff Butler<sup>c</sup>, Ian G. Barr<sup>c,d</sup>, Jodie McVernon<sup>a,e</sup>, Aeron C. Hurt<sup>c,d</sup>, James M. McCaw<sup>a,e,f,\*</sup>

<sup>a</sup> Melbourne School of Population and Global Health, The University of Melbourne, Parkville, Victoria, Australia

<sup>b</sup> Centre for Transformative Innovation, Swinburne University of Technology, Hawthorn, Victoria, Australia

<sup>c</sup> WHO Collaborating Centre for Reference and Research on Influenza, Victorian Infectious Diseases Reference Laboratory at the Peter Doherty Institute for Infection and Immunity, Melbourne, Victoria, Australia

<sup>d</sup> School of Applied Sciences, Monash University, Churchill, Victoria, Australia

<sup>e</sup> Murdoch Childrens Research Institute, The Royal Children's Hospital, Parkville, Victoria, Australia

<sup>f</sup> School of Mathematics and Statistics, The University of Melbourne, Parkville, Victoria, Australia

## HIGHLIGHTS

- Influenza viral fitness can be probed using *in vivo* co-infection experiments.
- We use a within-host model of such experiments to quantify relative fitness.
- Different assumptions for the biological cause of fitness difference are explored.
- Certain neuraminidase mutations enhance the fitness of drug-resistant influenza.
- Our findings are consistent regardless of the assumed cause of fitness difference.

## ARTICLE INFO

### Article history:

Received 9 January 2015

Received in revised form

2 July 2015

Accepted 6 July 2015

Available online 15 July 2015

### Keywords:

Influenza

Mathematical model

Viral kinetics

Drug-resistance

Pathogen fitness

## ABSTRACT

Through accumulation of genetic mutations in the neuraminidase gene, the influenza virus can become resistant to antiviral drugs such as oseltamivir. Quantifying the fitness of emergent drug-resistant influenza viruses, relative to contemporary circulating viruses, provides valuable information to complement existing efforts in the surveillance of drug-resistance. We have previously developed a co-infection based method for the assessment of the relative *in vivo* fitness of two competing viruses. We have also introduced a model of within-host co-infection dynamics that enables relative within-host fitness to be quantified in these competitive-mixtures experiments. The model assumed that fitness differences between co-infecting strains were mediated by strain-dependent viral production rates from infected epithelial cells. Here we extend the model to enable a more complete exploration of biological processes that may differ between virus pairs and hence generate fitness differences. We use the extended model to re-analyse data from competitive-mixtures experiments that investigated the fitness of oseltamivir-resistant (OR) H1N1 pandemic 2009 ("H1N1pdm09") viruses that emerged during a community outbreak in Australia in 2011. Results are consistent with those of our previous analysis, suggesting that the within-host replication fitness of these OR viruses is not compromised relative to that of related oseltamivir-susceptible (OS) strains, and that potentially permissive mutations in the neuraminidase gene (V241I and N369K) significantly enhance the fitness of H1N1pdm09 OR viruses. These results are consistent regardless of the hypothesised biological cause of fitness difference.

© 2015 Elsevier Ltd. All rights reserved.

## 1. Introduction

Antiviral drugs are used to treat influenza infection and reduce the onward spread of infection (Nicholson et al., 2003; Sullivan et al., 2010; Grienke et al., 2012). Currently circulating influenza viruses are predominantly susceptible to the neuraminidase (NA) inhibitor oseltamivir, however the drug's utility as a treatment

\* Corresponding author at: Melbourne School of Population and Global Health, The University of Melbourne, Parkville, Victoria, Australia.

E-mail address: [jamesm@unimelb.edu.au](mailto:jamesm@unimelb.edu.au) (J.M. McCaw).

option for influenza may be severely compromised if resistance becomes prevalent (Kelso and Hurt, 2012). During the Northern Hemisphere's 2007/08 influenza season, surveillance studies identified a rise in the proportion of A(H1N1) viruses carrying the resistance-conferring H275Y mutation in the NA gene (Sheu et al., 2008; Centers for Disease Control and Prevention (CDC), 2008; Hauge et al., 2009; Meijer et al., 2009). These resistant viruses spread globally and replaced wild-type H1N1 during 2008 (Centers for Disease Control and Prevention (CDC), 2009; Dharan et al., 2009; Hurt et al., 2009; Moscona, 2009), largely independently of the use of oseltamivir (Dharan et al., 2009; Hauge et al., 2009; Hurt et al., 2009; Meijer et al., 2009). This event highlighted a need to be able to accurately assess the relative fitness of emergent drug-resistant influenza strains compared to contemporary circulating drug-susceptible wild-type strains.

Previous studies have quantified the relative replication fitness of different pathogens using mathematical models (Marée et al., 2000; Wu et al., 2006; Hurt et al., 2010; Holder et al., 2011; Pinilla et al., 2012; Butler et al., 2014). A method introduced by Marée et al. (2000) quantified relative *in vitro* fitness via the ratio of the infected cell replication rates of each competing strain. Marée et al. discussed alternatives to their assumption that the replication rate is the only parameter that differs by strain (e.g. the infected cell death rate could instead be assumed to be the source of strain difference), however other possible biological sources of strain difference were not considered, such as strain-dependence in the latent phase duration. Wu et al. (2006) quantified relative *in vitro* fitness using the overall growth rate for each strain. This method is difficult to compare across different experiments because the growth rate incorporates the number of target cells, and so changes depending on experimental conditions. Wu et al. also did not consider alternative scenarios regarding the source of strain difference. In earlier work (Hurt et al., 2010), we quantified relative *in vivo* fitness via the difference of the infected cell replication rates of each strain. However, we neglected other possible causes of strain difference, such as strain-dependence in the duration of either the latent or productive phase of infected cells. Holder et al. (2011) and Pinilla et al. (2012) quantified relative *in vitro* fitness by estimating several fundamental biological properties of each strain, gaining direct insight into the underlying cause of strain-dependent infection dynamics and fitness differences. Quantifying relative fitness in this way is preferable to estimating experiment-specific properties that change depending upon modifications to the infection system (e.g. Wu et al., 2006), and depending on the biological properties of the pathogens being studied, may also be preferable to assuming that the infected cell replication rate or death rate are the only parameters that differ by strain (e.g. Marée et al., 2000).

In a recent experimental study involving the co-infection of animals with competing pairs of A(H1N1) pandemic 2009 ("H1N1pdm09") strains (Butler et al., 2014), we used a within-host model of the co-infection system to quantify relative replication fitness. The model assumed that fitness differences were caused by strain-dependence in the production rate of infectious virus by infected cells, and relative within-host fitness was quantified via the ratio of the production rates. Results indicated that (1) H275Y drug-resistant influenza viruses that emerged in 2011 in the Hunter New England (HNE) region of New South Wales, Australia, did not have compromised *in vivo* fitness compared with related drug-sensitive viruses, and (2) the unusually robust fitness of these drug-resistant viruses may have been due to the presence of two permissive NA mutations – V241I and N369K – which have since become established in virtually all circulating H1N1pdm09 viruses. Here we first revisit the model introduced in Butler et al. (2014), and then extend it to allow investigation of several different biologically plausible hypotheses

regarding the cause of fitness difference. Of note, our focus throughout the analysis is to obtain accurate and precise estimates for the relative fitness, rather than individual model parameters.

## 2. Experimental data

We analyse data from a competitive-mixtures experimental study involving co-infection of ferrets with pairs of competing influenza viruses (Butler et al., 2014). In these experiments, immunologically naive ferrets were inoculated with various mixtures of two different influenza strains ("A" and "B"). Each ferret was assigned either to one of three "mixed-infection groups" (80A:20B, 50A:50B, and 20A:80B), or to one of two "pure-infection groups" (100A:0B and 0A:100B). Each inoculum was prepared at the required proportion by combining known concentrations of each virus.

Nasal wash samples were taken daily from each ferret. The infectious viral load of each sample was measured using 50% tissue culture infectious dose (TCID<sub>50</sub>) assays, and total (infectious + non-infectious) viral load was measured using real-time reverse transcription-polymerase chain reaction (rRT-PCR) assays of the matrix gene. The proportion of each co-infecting virus was also measured using pyrosequencing assays of the NA gene of each co-infecting strain. Dynamics in this vRNA proportion over the course of infection provide insight into relative replication fitness within the mixed-infection groups. Differences in viral load dynamics between the two pure-infection groups also provide insight into relative replication fitness. Pyrosequencing and rRT-PCR measurements were taken for each inoculum.

Reverse genetics techniques were used to generate drug-resistant viruses with or without certain potentially permissive NA mutations – V241I and N369K – that were hypothesised to have counteracted the fitness cost of the H275Y mutation. The different virus pairs investigated in each competitive-mixtures experiment are shown in Table 1, and full details of the experimental procedures have previously been presented (Butler et al., 2014).

## 3. Within-host co-infection model

Epithelial cells infected with influenza produce both infectious and non-infectious virus. In order to model competitive-mixtures experiments, we extended our previous model of infectious and non-infectious influenza viral dynamics (Petrie et al., 2013) to incorporate two different co-infecting strains (Butler et al., 2014). This "co-infection" model (Fig. 1) assumes that target cells (*T*) may be infected by either strain A ( $V_A^{TCID}$ ) or strain B ( $V_B^{TCID}$ ) infectious virions; i.e. each strain competes for the same target cell resources (Butler et al., 2014):

$$\frac{dT}{dt} = -\beta_A TV_A^{TCID} - \beta_B TV_B^{TCID}. \quad (1)$$

For each strain, infected target cells progress through a latent phase (*L*) before becoming infectious (*I*) as described by the following equations (Butler et al., 2014):

$$\frac{dL_A}{dt} = \beta_A TV_A^{TCID} - k_A L_A$$

$$\frac{dL_B}{dt} = \beta_B TV_B^{TCID} - k_B L_B$$

$$\frac{dI_A}{dt} = k_A L_A - \delta_A I_A$$

$$\frac{dI_B}{dt} = k_B L_B - \delta_B I_B$$

**Table 1**

Virus pairs analysed in Butler et al. (2014). Each row shows the virus pair (“A” vs. “B”) analysed in a given competitive-mixtures experiment, together with a description of each virus. One experiment involved naturally isolated viruses (row 1) while the other experiments involved viruses generated using reverse genetics (rg) techniques (rows 2–5). All oseltamivir-resistant (OR) viruses contained the H275Y NA mutation (tyrosine (Y) at position 275), whereas the oseltamivir-susceptible (OS) virus did not contain that mutation (histidine (H) at position 275).

A	B	Description
New17 OR	New163 OS	An OR virus isolated from the HNE outbreak (A/Newcastle/17/2011), paired with an OS wild-type virus isolated during the same outbreak (A/Newcastle/163/2011).
rgNew17 OR	rgNew17 I241V OR	A virus genetically identical to the New17 OR isolate which naturally encodes the V241I and N369K NA substitutions (rgNew17 OR), paired with the same virus except with V241I removed (rgNew17 I241V OR).
rgNew17 OR	rgNew17 K369N OR	The rgNew17 OR virus, paired with the same virus except with N369K removed (rgNew17 K369N OR).
rgNew17 OR	rgNew17 K369N, I241V OR	The rgNew17 OR virus, paired with the same virus except with both V241I and N369K removed (rgNew17 I241V, K369N OR).
rgPerth261 N369K, V241I OR	rgPerth261 OR	A virus genetically identical to an early (2009) OR isolate, A/Perth/261/2009, which does not naturally encode the V241I and N369K NA substitutions (rgPerth261 OR), paired with the same virus except containing the V241I and N369K mutations (rgPerth261 V241I, N369K OR).

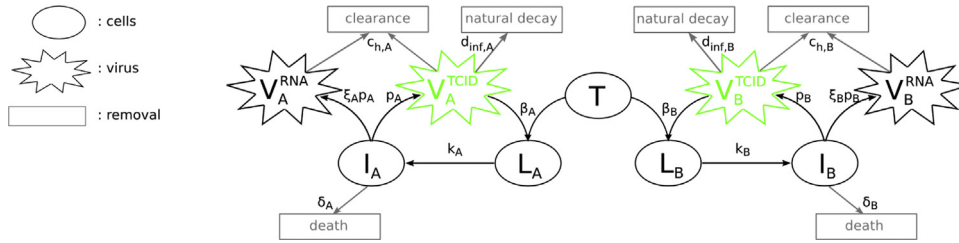


**Fig. 1.** Co-infection model. For each strain, infectious virions ( $V^{TCID}$ ) infect target cells ( $T$ ) which, following a latent phase ( $L$ ), become productively infected ( $I$ ) and release both infectious ( $V^{TCID}$ ) and total ( $V^{RNA}$ ) virions. Infectious virions naturally decay into non-infectious virions, and we assume that the natural decay process does not affect vRNA concentration as measured by rRT-PCR assays. Host-driven clearance affects all viral particles.  $V^{TCID}_{comb} = V^{TCID}_A + V^{TCID}_B$ ,  $V^{RNA}_{comb} = V^{RNA}_A + V^{RNA}_B$ , and  $V^{RNA}_B = V^{RNA}_B / V^{RNA}_{comb}$  are fitted to TCID<sub>50</sub>, rRT-PCR, and pyrosequencing data, respectively. For clarity, the colours of the  $V^{TCID}_A$ ,  $V^{TCID}_B$ ,  $V^{RNA}_A$ , and  $V^{RNA}_B$  compartments (green/black) are matched to the colours of the corresponding viral load curves in Fig. 2. Adapted from the Supplementary Text of Butler et al. (2014). (For interpretation of the references to color in this figure caption, the reader is referred to the web version of this paper.)

$$\begin{aligned}
 \frac{dV_A^{TCID}}{dt} &= p_A I_A - c_{h,A} V_A^{TCID} - d_{inf,A} V_A^{TCID} \\
 \frac{dV_B^{TCID}}{dt} &= p_B I_B - c_{h,B} V_B^{TCID} - d_{inf,B} V_B^{TCID} \\
 \frac{dV_A^{RNA}}{dt} &= \xi_A p_A I_A - c_{h,A} V_A^{RNA} \\
 \frac{dV_B^{RNA}}{dt} &= \xi_B p_B I_B - c_{h,B} V_B^{RNA}
 \end{aligned} \quad (2)$$

Details of all state variables and parameters in this model are shown in Table 2, together with fixed parameter values and the biologically realistic bounds used to constrain fitted parameters. In order to produce more biologically accurate distributions for the latent and infected cell lifespans, the  $L$  and  $I$  compartments are each split into 20 stages, for both strain A and strain B (Petrie et al., 2013). The model is similar to that used by Pinilla et al. (2012) to model competition between co-infecting strains in cell culture.

#### 4. Fitting the model to data

When fitting model outputs to experimental data, three different assay types are used:

1. the infectious virus concentration of both strains combined ( $V^{TCID}_{comb} = V^{TCID}_A + V^{TCID}_B$ ) is fitted to TCID<sub>50</sub> data;
2. the viral RNA concentration of both strains combined ( $V^{RNA}_{comb} = V^{RNA}_A + V^{RNA}_B$ ) is fitted to rRT-PCR data;
3. the proportion of viral RNA comprised of strain B ( $V^{RNA}_B / V^{RNA}_{comb}$ ) is fitted to pyrosequencing data.

TCID<sub>50</sub> data were obtained using several separate runs of the assays in Butler et al. (2014) (due to the limited number of samples able to be tested with any single assay), and inter-assay variability was controlled for by including, in each assay, 1–2 samples from

stocks of control virus. We use these control samples to calibrate all TCID<sub>50</sub> data. Each measurement in a given assay is scaled up by adding, in log-space, the difference between that assay's average calibration value and the largest average calibration value obtained across all TCID<sub>50</sub> assays in all experiments.

Initial conditions for  $T$ ,  $L$ ,  $I$ , and  $V^{TCID}_{comb}$  are identical to those used in our previous within-host modelling study of ferret infection (Petrie et al., 2013), i.e.  $T(0) = 7 \times 10^7$ ,  $L(0) = I(0) = 0$  (for each strain), and  $V^{TCID}_{comb}(0)$  is a fitted parameter. For each infection group the initial proportion of infectious virus comprised of strain B ( $V^{TCID}_B(0) / V^{TCID}_{comb}(0)$ ) is fixed to the proportion prepared in the inoculum. The initial total:infectious ratio for both strains combined ( $\rho(0) = V^{RNA}_{comb}(0) / V^{TCID}_{comb}(0)$ ) is fitted to the rRT-PCR:TCID<sub>50</sub> ratio as measured in the inoculum. Measurements of the rRT-PCR:TCID<sub>50</sub> ratio varied systematically across the different mixed inocula, indicating that the two competing strains in a given experiment may have had different ratios. We assume that  $\rho(0)$  is strain-dependent, introducing  $\rho_A(0)$  and  $\rho_B(0)$  as follows:

$$\begin{aligned}
 \rho(0) &= \frac{V^{RNA}_{comb}(0)}{V^{TCID}_{comb}(0)} = \frac{V^{RNA}_A(0) + V^{RNA}_B(0)}{V^{TCID}_{comb}(0)} \\
 &= \frac{\rho_A(0) V^{TCID}_A(0) + \rho_B(0) V^{TCID}_B(0)}{V^{TCID}_{comb}(0)} \\
 &= \rho_A(0) \left( 1 - \frac{V^{TCID}_B(0)}{V^{TCID}_{comb}(0)} \right) + \rho_B(0) \frac{V^{TCID}_B(0)}{V^{TCID}_{comb}(0)}.
 \end{aligned} \quad (3)$$

The initial proportion of total virus comprised of strain B ( $V^{RNA}_B(0) / V^{RNA}_{comb}(0)$ ) is fitted to inoculum pyrosequencing data.

For pure-infection group ferrets, the strain omitted from each group's inoculum is assumed to be absent throughout the entire course of infection. Those data are fitted with only a single strain present in the model. This assumption is supported by an inspection of the raw data (Butler et al., 2014), which suggest that the

**Table 2**

*Co-infection model states and parameters.* Descriptions of all state variables (compartments) and parameters in the co-infection model (most descriptions are reproduced from the Supplementary Text of [Butler et al. \(2014\)](#)). Biologically realistic lower and upper bounds for each fitted parameter are also shown; these are used to restrict parameters to realistic values during fitting.

Parameter	Description	Units	Fixed value	Fitting bounds	Source <sup>a</sup>
$T$	Number of target cells	cells	–	–	–
$T(0)$	Initial $T$ value	cells	$7 \times 10^7$	–	This estimate was calculated in our previous within-host modelling study of ferret infection ( <a href="#">Petrie et al., 2013</a> ).
$L$	Number of latently infected cells	cells	–	–	–
$L(0)$	Initial $L$ value	cells	0	–	–
$I$	Number of productively infected cells	cells	–	–	–
$I(0)$	Initial $I$ value	cells	0	–	–
$V^{TCID}$	Concentration of free infectious virions measured via TCID <sub>50</sub> infectivity assay	TCID <sub>50</sub> /ml of nasal wash	–	–	–
$V^{TCID}(0)$	Initial $V^{TCID}$ concentration	TCID <sub>50</sub> /ml	–	$[10^{-6}, 10^{4.699}]$	Upper bound based on a scenario in which <i>all</i> infectious virus in each inoculum given to donor ferrets – i.e. $10^{4.699}$ TCID <sub>50</sub> – is taken up into the URT. Hypothetically, if a nasal wash sample had been taken from a donor immediately after inoculation, it would be impossible for there to be more than $10^{4.699}$ TCID <sub>50</sub> within the 1 ml of solution that is used in such a nasal wash. Lower bound based on a previous theoretical estimate of the lowest possible TCID <sub>50</sub> value that corresponds to a single infectious virion in the URT ( <a href="#">Petrie et al., 2013</a> ).
$V^{RNA}$	Concentration of free vRNA (present in both infectious and non-infectious virus) measured via RT-PCR assay	vRNA copies/ml	–	–	–
$p$	Production rate of infectious virions	(TCID <sub>50</sub> /ml) cell <sup>-1</sup> d <sup>-1</sup>	–	$[10^{-4}, 10^2]$	Previous <i>in vivo</i> and <i>in vitro</i> modelling estimates of $p$ ( <a href="#">Möhler et al., 2005</a> ; <a href="#">Baccam et al., 2006</a> ; <a href="#">Handel et al., 2007</a> ; <a href="#">Beauchemin et al., 2008</a> ; <a href="#">Schulze-Horsel et al., 2009</a> ; <a href="#">Miao et al., 2010</a> ; <a href="#">Saenz et al., 2010</a> ; <a href="#">Holder and Beauchemin, 2011</a> ; <a href="#">Smith et al., 2011</a> ; <a href="#">Pawelek et al., 2012</a> ).
$\beta$	Infectivity/mixing rate governing infection of target cells by infectious virions	(TCID <sub>50</sub> /ml) <sup>-1</sup> d <sup>-1</sup>	–	$[10^{-9}, 10^{-1}]$	Previous <i>in vivo</i> and <i>in vitro</i> modelling estimates of $\beta$ ( <a href="#">Möhler et al., 2005</a> ; <a href="#">Baccam et al., 2006</a> ; <a href="#">Handel et al., 2007</a> ; <a href="#">Beauchemin et al., 2008</a> ; <a href="#">Schulze-Horsel et al., 2009</a> ; <a href="#">Miao et al., 2010</a> ; <a href="#">Saenz et al., 2010</a> ; <a href="#">Smith et al., 2011</a> ; <a href="#">Pawelek et al., 2012</a> ).
$k$	Transition rate from latent to productive infection	d <sup>-1</sup>	–	[1, 24]	This range corresponds to average latently infected cell lifetimes (i.e. $\tau_L = 1/k$ ) from 1 h to 24 h, consistent with previous estimates obtained when fitting models (with normal or log-normal delay distributions for $L$ and $I$ ) to <i>in vitro</i> data ( <a href="#">Holder and Beauchemin, 2011</a> ; <a href="#">Holder et al., 2011</a> ; <a href="#">Pinilla et al., 2012</a> ).
$\delta$	Death rate of productively infected cells	d <sup>-1</sup>	–	[0.24, 8]	This range corresponds to average productively infected cell lifetimes (i.e. $\tau_I = 1/\delta$ ) from 3 h to 100 h, consistent with previous <i>in vitro</i> observations ( <a href="#">Arndt et al., 2002</a> ; <a href="#">Zhirnov and Klenk, 2003</a> ; <a href="#">Möhler et al., 2005</a> ) as well as both <i>in vivo</i> and <i>in vitro</i> model-fitting estimates ( <a href="#">Möhler et al., 2005</a> ; <a href="#">Baccam et al., 2006</a> ; <a href="#">Handel et al., 2007</a> ; <a href="#">Beauchemin et al., 2008</a> ; <a href="#">Schulze-Horsel et al., 2009</a> ; <a href="#">Miao et al., 2010</a> ; <a href="#">Holder and Beauchemin, 2011</a> ; <a href="#">Smith et al., 2011</a> ; <a href="#">Pinilla et al., 2012</a> ).
$c_h$	Host-driven clearance rate (assumed to be the same for both infectious and non-infectious virus)	d <sup>-1</sup>	–	$[10^{-2}, 10^3]$	Previous <i>in vivo</i> estimates for the clearance rate of infectious virions obtained from target cell-limited models (where infection progress is limited by the availability of susceptible cells, rather than by immune response dynamics) ( <a href="#">Baccam et al., 2006</a> ; <a href="#">Handel et al., 2007</a> ; <a href="#">Miao et al., 2010</a> ; <a href="#">Holder and Beauchemin, 2011</a> ; <a href="#">Smith et al., 2011</a> ) <sup>b</sup>
$d_{inf}$	Degradation rate of infectious virus to non-infectious virus	d <sup>-1</sup>	3.12	–	Consistent with the rate of loss of infectivity determined <i>in vitro</i> for two H1N1pdm09 strains ( <a href="#">Pinilla et al., 2012</a> ). This value is also consistent with other <i>in vitro</i> measurements ( <a href="#">Horsfall, 1954</a> ; <a href="#">Paucker and Henle, 1955</a> ; <a href="#">Gaush and Smith, 1968</a> ; <a href="#">Orthel, 1972</a> ; <a href="#">Beauchemin et al., 2008</a> ; <a href="#">Schulze-Horsel et al., 2009</a> ; <a href="#">Holder et al., 2011</a> ).
$\xi$	Ratio of total vRNA measured via rRT-PCR to infectious virions measured via TCID <sub>50</sub> , as produced by infected cells	vRNA copies/TCID <sub>50</sub>	–	$[10^0, 10^6]$	Based on the variability of the rRT-PCR:TCID <sub>50</sub> ratio within the <a href="#">Butler et al. (2014)</a> data.
$\rho(0)$	Initial total:infectious ratio for both strains combined ( $\rho(0) = V_{comb}^{RNA}(0)/V_{comb}^{TCID}(0)$ )	vRNA copies/TCID <sub>50</sub>	–	$[10^0, 10^5]$	Based on the variability of $\rho(0)$ across different inocula given to donor ferrets in <a href="#">Butler et al. (2014)</a> .

<sup>a</sup> For reviews of parameter estimates obtained by within-host modelling influenza studies, see [Smith and Perelson \(2011\)](#) and [Beauchemin and Handel \(2011\)](#).

<sup>b</sup> Note that previous estimates of the infectious virus clearance rate (usually referred to as  $c$ ) implicitly include both  $c_h$  and  $d_f$ ; hence we expect  $c_h$  to be somewhat smaller than previous estimates of  $c$ .

probability of spontaneous mutation from one strain to the other is low throughout the course of a pure infection. Data from mixed-infection group ferrets are fitted with the full two-strain version of the model.

Measurements that are outside detection thresholds are fitted as previously explained ([Petrie et al., 2013](#)). Pyrosequencing measurements are considered to be outside the threshold of detectability when they are outside the range [0.02, 0.98], as the



pyrosequencing error for each experiment was generally around 2%.

Model parameters are estimated by minimising the sum of squared residuals (SSR) between model outputs and data, using a similar method to previous within-host modelling studies (Saenz et al., 2010; Petrie et al., 2013). For a single set of model parameters ( $\theta$ ) the SSR is

$$\begin{aligned} \text{SSR}(\theta) = & \sum_{i=1}^{N_{\text{TCID}}} \left( \frac{\log_{10} \hat{V}_i^{\text{TCID}} - \log_{10} V_{\text{comb}}^{\text{TCID}}(t_i, \theta)}{\log_{10} \hat{V}_{\text{max}}^{\text{TCID}} - \log_{10} \hat{V}_{\text{thr}}^{\text{TCID}}} \right)^2 \\ & + \sum_{i=1}^{N_{\text{PCR}}} \left( \frac{\log_{10} \hat{V}_i^{\text{PCR}} - \log_{10} V_{\text{comb}}^{\text{RNA}}(t_i, \theta)}{\log_{10} \hat{V}_{\text{max}}^{\text{PCR}} - \log_{10} \hat{V}_{\text{thr}}^{\text{PCR}}} \right)^2 \\ & + \sum_{i=1}^{N_{\rho(0)}} \left( \frac{\log_{10} \hat{\rho}_i(0) - \log_{10} \rho(0, \theta)}{\log_{10} \hat{\rho}_{\text{max}}(0) - \log_{10} \hat{\rho}_{\text{min}}(0)} \right)^2 \\ & + \sum_{i=1}^{N_{\text{pyro}}} \left( \hat{V}_{B,i}^{\text{pyro}} - V_B^{\text{RNA}}(t_i, \theta) \right)^2, \end{aligned} \quad (4)$$

where  $N_{\text{TCID}}$ ,  $N_{\text{PCR}}$ ,  $N_{\rho(0)}$ , and  $N_{\text{pyro}}$  are the number of TCID<sub>50</sub>, rRT-PCR,  $\hat{\rho}(0)$  (i.e. rRT-PCR/TCID<sub>50</sub>), and pyrosequencing data points being fitted, respectively;  $t_i$  is the time that the  $i$ th data point was measured;  $\hat{V}_i^{\text{TCID}}$ ,  $\hat{V}_i^{\text{PCR}}$ ,  $\hat{\rho}_i(0)$ , and  $\hat{V}_{B,i}^{\text{pyro}}$  denote the  $i$ th measurement for each respective assay;  $\hat{V}_{\text{max}}^{\text{TCID}}$ ,  $\hat{V}_{\text{max}}^{\text{PCR}}$ , and  $\hat{\rho}_{\text{max}}(0)$  are the maximum values that were obtained (for the particular experiment being fitted) across all TCID<sub>50</sub>, rRT-PCR, and  $\hat{\rho}(0)$  measurements, respectively;  $\hat{\rho}_{\text{min}}(0)$  is the minimum value that was obtained across all  $\hat{\rho}(0)$  measurements; and  $\hat{V}_{\text{thr}}^{\text{TCID}}$  and  $\hat{V}_{\text{thr}}^{\text{PCR}}$  denote detection thresholds for each respective assay.

MATLAB 2011b's genetic algorithm (GA) is used to ensure that a good candidate for the global minimum of the SSR is obtained and to generate likelihood confidence regions (LCRs) and confidence intervals (CIs) for parameter estimates, as detailed previously (Petrie et al., 2013; Schwaab et al., 2008; Donaldson and Schnabel, 1987). The rate of degradation of infectious to non-infectious virus is fixed to  $d_{\text{inf}} = 3.12 \text{ d}^{-1}$ ; a value estimated previously *in vitro* for two H1N1pdm09 viruses (Pinilla et al., 2012). This value is also consistent with other *in vitro* measurements (Horsfall, 1954; Paucker and Henle, 1955; Gaush and Smith, 1968; Orthel, 1972; Beauchemin et al., 2008; Schulze-Horsel et al., 2009; Holder et al., 2011). For all fitted parameters in the co-infection model, a range of biologically plausible values are specified (Table 2) which restrict the parameter space searchable by the GA. Different hypothesised models are compared statistically using the Akaike information criterion (AIC) in the case of least squares estimation with normally distributed errors (Burnham and Anderson, 2004). The AIC corrected for datasets with few data points (AIC<sub>c</sub>) is used.

## 5. Quantifying relative fitness using ratios of strain-dependent model parameters

Once model parameters have been estimated for each competing strain, relative replication fitness is quantified via the ratio of each pair of strain-dependent parameters. As the underlying biological cause of experimentally observed strain-dependence in infection dynamics is unknown and may differ depending on which two strains are being compared, we investigate several different hypotheses regarding the biological processes that may differ (Section 6). To avoid parameter identifiability issues, each hypothesis is investigated separately by allowing one biological parameter to be strain-dependent at a time, while all other biological parameters are assumed to be equivalent for both

strains. Note that  $\rho(0)$  is also assumed to be strain-dependent (see Section 4), however that parameter is simply an initial condition of the infection system which is affected by each virus' storage conditions leading up to a given experiment, rather than a fundamental biological property of each virus.

For each hypothesis, strain-dependence in the associated biological parameter generates a fitness difference between strains. Relative fitness is quantified via the ratio of these two strain-dependent parameters. An estimated value of one for the ratio indicates equivalent fitness between the two strains; values on either side of one indicate greater or lesser fitness, driven by differences in the parameter under study.

## 6. Hypothesised explanations for a fitness difference between strains that have distinct NA genes

In the competitive-mixtures experiments analysed here (Table 1) co-infecting viruses differ (primarily or solely) via mutations in the NA gene. Hence the hypothesised causes for a fitness difference that we choose to investigate are informed by previous *in vitro* experiments that examined functions of influenza NA ((Colman, 1994; Gubareva et al., 2000; Wagner et al., 2002; Nayak et al., 2004; Gong et al., 2007; Rossman and Lamb, 2011; Yondola et al., 2011; Lai et al., 2010; Ushirogawa and Ohuchi, 2011; Matrosovich et al., 2004; de Vries et al., 2012; Gerlach et al., 2012; Nishikawa et al., 2012; Wong et al., 2012; Hatrup and Gendler, 2008; Thornton et al., 2008; Suzuki et al., 2005; Su et al., 2009; Zhu et al., 2012; Morris et al., 1999; Gaur et al., 2012; Huang et al., 2008); summarised in Appendix A).

### 6.1. The $p$ -diff model

Previous *in vitro* work has indicated the importance of NA in the production of free virions, and in regulating the balance of infectious and non-infectious virions during production from infected cells (see Appendix A). One hypothesis we investigate is that the production rate of infectious virus ( $p$ ) differs between strains while all other rate parameters are identical for both strains; hence *relative fitness* =  $p_B/p_A$ . This assumption was made in our previous analysis of these experiments (Butler et al., 2014). We refer to the resulting model as the “ $p$ -diff” model. Under the  $p$ -diff model, a larger estimated value for  $p$  indicates greater replication fitness, as a greater rate of production of infectious virus leads to a greater exponential growth rate for infectious virus and infected cells (assuming that target cells are available for infection once progeny virus production begins).

### 6.2. The $\beta$ -diff model

Previous experimental results have indicated that NA is important for virus entry into susceptible cells (see Appendix A). Other *in vitro* work has also indicated that NA is important in counteracting the effects of decoy receptors in mucins that (1) restrict the spatial spread of free virus throughout the site of infection, and (2) clear free virus (see Appendix A).

To account for the first of these mucin-counteracting functions of NA, as well as the possibility that NA may affect the infectivity of each infectious virion, we investigate a hypothesis that only the infectivity/mixing rate ( $\beta$ ) differs between strains (the “ $\beta$ -diff” model), where *relative fitness* =  $\beta_B/\beta_A$ . This hypothesis embodies a scenario in which NA counteracts the inhibition of the spatial spread of free virus, and/or alters the infectivity of infectious virions, in a strain-dependent manner. Under the  $\beta$ -diff model, a larger estimated value for  $\beta$  indicates greater replication fitness, as faster spatial spread of infectious virus and/or greater infectivity

per virion leads to a greater exponential growth rate for numbers of infected cells.

### 6.3. The $\tau_V$ -diff model

To account for the second of the previously mentioned mucin-counteracting functions of NA, we also investigate a hypothesis in which only host-driven clearance ( $c_h$ ) is strain-dependent. This embodies a scenario in which NA counteracts the host-driven clearance of free virus in a strain-dependent manner. Under this hypothesis, a larger estimated  $c_h$  rate indicates that virions are cleared more quickly from the site of infection, leading to a relatively decreased exponential growth rate in numbers of infected cells and a more rapid exponential decay rate for free virus. Larger  $c_h$  values are associated with decreased within-host fitness. To aid in presentation we therefore use an alternative parameterisation of host-driven clearance: strain-dependence in the expected lifetime of infectious virions ( $\tau_{Vinf} = 1/[c_h + d_{inf}]$ , with  $d_{inf}$  fixed); hence *relative fitness* =  $\tau_{Vinf,B}/\tau_{Vinf,A}$ . This hypothesised model is referred to as the “ $\tau_V$ -diff” model.

### 6.4. The $\tau_I$ -diff model

Other *in vitro* work has indicated that NA may be important in determining the lifetime of infected cells (see Appendix A), which in the co-infection model is dependent upon the average duration of both the latent phase ( $\tau_L = 1/k$ ) and productive phase ( $\tau_I = 1/\delta$ ). One way to incorporate this possible function of NA is to investigate a hypothesis in which only  $\delta$  is strain-dependent. Under this hypothesis, a larger estimated value for  $\delta$  indicates that infected cells produce infectious virus for shorter durations on average (shorter  $\tau_I$ ), leading to relatively lower amounts of free infectious virus, a decreased rate of exponential growth for infected cells (if there are still target cells available for infection once infected cells start dying), and more rapid reduction of infected cell numbers towards the end of infection. Larger  $\delta$  values are associated with decreased replication fitness. Similar to the  $\tau_V$ -diff model, to aid presentation relative fitness is quantified using the infected cell productive phase duration ( $\tau_I$ ) rather than death rate ( $\delta$ ); hence *relative fitness* =  $\tau_{I,B}/\tau_{I,A}$ .

### 6.5. The $k$ -diff model

As mentioned above in the context of the  $\tau_I$ -diff hypothesis, NA may be important in determining the lifetime of infected cells. Another way to account for this possible function of NA is to investigate a hypothesis in which only the transition rate from latent to productive infection ( $k$ ) differs between strains (the “ $k$ -diff” model), where *relative fitness* =  $k_B/k_A$ . Under this hypothesis, a larger estimated  $k$  value indicates that the average latent phase duration is shorter so infected cells initiate production of infectious virus more quickly, leading to an increased rate of exponential growth for both infected cells (if there are still target cells available for infection once progeny virus production begins) and infectious virus. Larger  $k$  values are associated with increased within-host fitness. This hypothesis is also supported by experimental results indicating that NA is important in the release of progeny virions from the surface of infected cells (see Appendix A).

## 7. The relative within-host replication fitness of an OR strain isolated during the HNE outbreak

Here we quantify the relative replication fitness of the New17 OR and New163 OS viruses isolated from the HNE outbreak (see

Table 1, row 1). We refer to this competitive-mixtures experiment as the natural isolate experiment.

### 7.1. Fits to data using the $p$ -diff hypothesis

Given that virus particle release from infected cells is often considered to be the primary function of NA, we first present our analyses of the  $p$ -diff model, in which strain-dependence in the production rate of infectious virus is hypothesised to be the underlying cause of fitness difference. All analyses performed using the  $p$ -diff model are identical to those presented in Butler et al. (2014). Fig. 2 shows fits of the  $p$ -diff model to TCID<sub>50</sub>, rRT-PCR, and pyrosequencing data from hosts in the natural isolate experiment (Butler et al., 2014). Fits of the other four hypothesised models to the natural isolate experiment are shown in Supplementary Figs. S2–S5.

Note that the pyrosequencing proportion data in the inocula of the natural isolate experiment are systematically lower than the proportions that were prepared according to TCID<sub>50</sub> mix (Fig. 2, centre column, blue squares at  $t=0$ ). Also the rRT-PCR:TCID<sub>50</sub> ratio measured in the inocula (right column, black dots at  $t=0$ ) increases systematically across the different infection groups with increasing New163 OS inoculum proportions, suggesting that the New163 OS isolate had a larger ratio of *total vRNA:infectious virus* compared with the New17 OR isolate. The co-infection model is able to reproduce each of these systematic effects by assuming that the initial *total vRNA:infectious virus* ratio in the inoculum ( $\rho(0)$ ) differs by strain, as discussed further in Section 9.

TCID<sub>50</sub> and rRT-PCR viral load generally decrease over time in the natural isolate experiment, with TCID<sub>50</sub> reaching undetectable levels by  $t \approx 6$ – $7$  :  $d$  (post-infection; *p.i.*) (Fig. 2, left column). Comparing the two pure-infection groups, there are no substantial differences in TCID<sub>50</sub> or rRT-PCR viral load dynamics between each group.

In the three mixed-infection groups, there is a general trend for the New17 OR pyrosequencing proportion (Fig. 2, centre column) to increase relative to its value in the inoculum (at  $t=0$ ); i.e. the New17 OR virus tends to outgrow the New163 OS virus within hosts. The slope of this increase also appears to become steeper with greater amounts of New163 OS virus in the inoculum. This trend is reproduced by the best-fit of the  $p$ -diff model (Fig. 2, solid blue line) but not by most other fits that lie within the 95% confidence level of the LCR (Fig. 2, faded dotted blue lines), which rapidly increase and then plateau prior to 24 h (*p.i.*). Note that this bimodality (i.e. two mechanistically distinct solutions that are each capable of reproducing observed infection dynamics) is a limitation of the  $p$ -diff model fitted to the natural isolate experiment, but does not typically occur for the other model-experiment combinations analysed in this work.

### 7.2. Fits to data using the four alternative hypotheses

Having analysed the natural isolate experiment using the  $p$ -diff model, we now analyse fits of the four other hypothesised models to that experiment:

- $\beta$ -diff (infectivity/mixing rate differs by strain),
- $\tau_V$ -diff (lifetime of infectious virions differs by strain),
- $\tau_I$ -diff (infected cell productive phase duration differs by strain),
- $k$ -diff (transition rate from latent to productive infection differs by strain).

Fits to infectious viral load, total viral load, and  $\rho(0)$  inoculum measurements are similar for all four models (Figs. S2–S5, left and right columns). However, fits to pyrosequencing data (Figs. S2–S5,

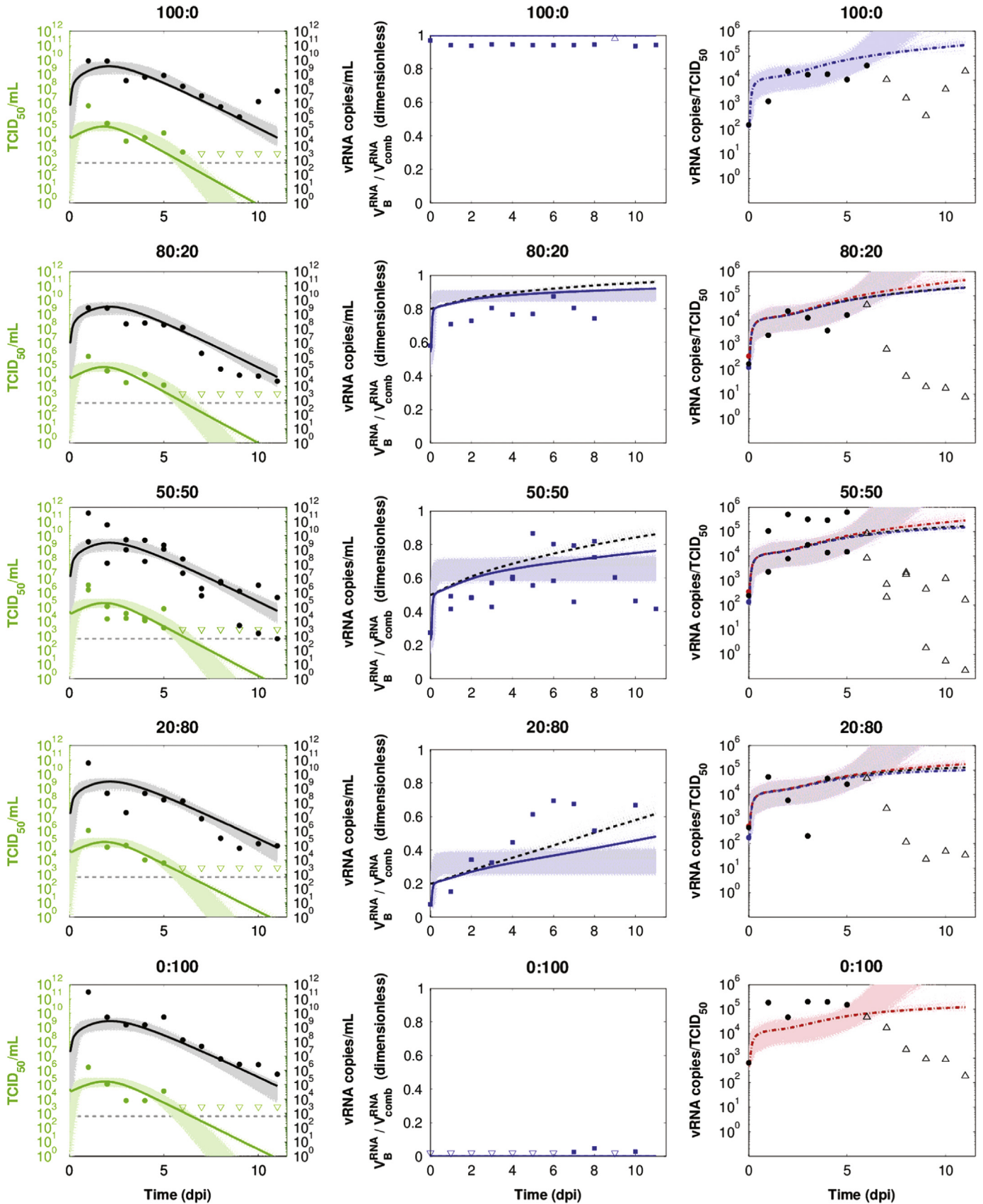


**Fig. 2.** Fits of the  $p$ -diff model to data from the natural isolate experiment. Each row shows viral load data for a given infection group. The 50:50 mixture was inoculated into two different ferrets in order to provide more data on infections that begin on equal footing; therefore data points may overlap in that group. *Left column:* Best fits are shown of infectious (solid green line;  $V_{\text{comb}}^{\text{TCID}}(t)$ ) and total (solid black line;  $V_{\text{comb}}^{\text{RNA}}(t)$ ) viral load to calibrated TCID<sub>50</sub> data (green dots) and rRT-PCR data (black dots; dashed grey line indicates detection threshold), respectively. *Centre column:* Best fits of the New17 OR vRNA proportion (solid blue line;  $V_{\text{B}}^{\text{RNA}}/V_{\text{comb}}^{\text{RNA}}$ ) to pyrosequencing data (blue squares). The New17 OR infectious proportion is also shown (dashed black line;  $V_{\text{B}}^{\text{TCID}}/V_{\text{comb}}^{\text{TCID}}$ ). *Right column:* Data of the rRT-PCR:TCID<sub>50</sub> ratio (black dots), together with the total:infectious ratio of both strains combined (dot-dashed black line;  $\rho(t) = V_{\text{B}}^{\text{RNA}}/V_{\text{comb}}^{\text{RNA}}(t)/V_{\text{comb}}^{\text{TCID}}(t)$ ). Note that only the initial condition,  $\rho(0)$ , is fitted to data. The total:infectious ratio of the New163 OS (dot-dashed red line; red dot indicates initial value) and New17 OR (dot-dashed blue line; blue dot indicates initial value) strains are also shown. In all plots, non-filled arrows indicate that the measured concentration or proportion was outside of the range of detectability for the corresponding assay, with arrow direction indicating the direction of the actual, unknown quantity. In addition to the best fit lines, 5000 randomly sampled fits with SSR values that lie within the 95% confidence level of the LCR are also shown (faded dotted lines). (For interpretation of the references to color in this figure caption, the reader is referred to the web version of this paper.)



centre column) exhibit different behaviours for different models, as does the predicted coupling between infectious and total A:B ratios. The infectious A:B ratio under the  $\tau_I$ -diff hypothesis (Fig. S4, dashed black line) decouples from the total vRNA A:B ratio (solid blue line) after  $t \approx 2\text{--}3$  d (p.i.). This decoupling is also present in some of the fits of the  $\tau_V$ - and  $k$ -diff hypotheses (as well as the  $p$ -diff hypothesis; Fig. 2), but does not occur under the  $\beta$ -diff hypothesis. The fact that predicted infectious proportion dynamics decouple from total vRNA proportion dynamics is crucial, because pyrosequencing assays measure the total vRNA proportion, yet infectious proportion dynamics provide a more direct insight into relative fitness. This highlights the importance of considering both infectious and total virus dynamics in competitive-mixtures experiments.

### 7.3. Differences in the ability of the five hypothesised models to reproduce observed infection dynamics

All models are able to generate some form of increase in the New17 OR vRNA proportion over time, yet certain models reproduce particular aspects of the pyrosequencing data better than others. The  $\beta$ -diff model is unable to generate the continual increase present in the pyrosequencing data from  $t = 0$  d(p.i.) to  $t \approx 6$  d(p.i.) (Fig. S2, centre column). Instead, the New17 OR vRNA proportion rapidly increases and then plateaus within the first 24 h (p.i.), similar to most of the fits generated using the  $p$ -diff model (Fig. 2, centre column). Both the  $p$ - and  $\tau_V$ -diff models are able to generate fits that reproduce the increase in vRNA proportion between  $t = 0$  d(p.i.) and  $t \approx 6$  d(p.i.) (Figs. 2 and S3, centre column). However, the vRNA proportion continues to increase beyond  $t \approx 6$  d(p.i.) in those fits, whereas the pyrosequencing data appear to plateau beyond  $t \approx 6$  d(p.i.) and perhaps even decrease following  $t \approx 8$  d(p.i.). The pyrosequencing dynamics in this final stage are, however, difficult to discern due to a relative lack of data following  $t \approx 8$  d(p.i.).

The  $\tau_I$ - and  $k$ -diff models are the most capable of reproducing all of the aforementioned features in the pyrosequencing data (Figs. S4 and S5, centre column), and are the best-fitting models overall for the natural isolate experiment. Each model's  $AIC_c$  value correlates well with its capacity to reproduce pyrosequencing data (Table 3), simply because model fits differ most prominently when fitting pyrosequencing data. However, these differences in the

ability of each hypothesised model to fit data are minor; our results do not provide strong evidence that any particular hypothesised model is more biologically plausible than the others. Table 4, row 1, provides a qualitative comparison of the performance of different models when fitting data from the natural isolate experiment.

### 7.4. Strain-dependent parameters are highly correlated

Estimates of strain-dependent parameters — e.g.  $p_{WT}$  for the OS wild-type strain and  $p_{MUT}$  for the OR mutant strain in the  $p$ -diff model — have a large degree of uncertainty and overlap. For example, this is evident in estimates of  $p_{WT}$  and  $p_{MUT}$  obtained when fitting the  $p$ -diff model to the natural isolate dataset (see Table 3 and Fig. S1 for all  $p$ -diff model parameter estimates and LCR projections, respectively).

Despite this uncertainty and overlap, which is present to some degree in all model-fits analysed in this work, each pair of strain-dependent parameters is generally highly correlated to the extent that their ratio is well estimated. This is evident in the LCR projection in Fig. 3, which shows the correlation of the two strain-dependent parameters in the  $p$ -diff model.

**Table 4**

*Model performance summary.* Qualitative comparison of the performance of each model when fitted to each experimental dataset. The symbols are to be interpreted as follows: ✓✓: best-fitting model(s) for a given dataset, which capture the trends in data well; ✓: good-fitting model(s) that capture the majority of trends in data; ? : marginal model(s) that, while plausible, reproduce some of the trends in data poorly; ×: poor model(s) that are implausible based on an inability to fit the data. Note that there is no reason to believe that the biological cause of fitness difference should be the same for different experiments.

Dataset	Hypothesised model				
	$p$ -diff	$\beta$ -diff	$\tau_V$ -diff	$\tau_I$ -diff	$k$ -diff
New17 OR vs. New163 OS	✓	?	✓	✓✓	✓✓
rgNew17 OR vs. rgNew17 I241V OR	✓✓	✓✓	✓	×	✓✓
rgNew17 OR vs. rgNew17 K369N OR	✓✓	✓	✓	?	✓
rgNew17 OR vs. rgNew17 K369N,I241V OR	✓	✓✓	?	✓	✓✓
rgPerth261 N369K,V241I OR vs. rgPerth261 OR	✓✓	✓✓	?	?	✓✓

**Table 3**

*$AIC_c$  values and estimates of fitted parameters and relative replication fitness, for the natural isolate experiment.* Best-fit estimates of relative within-host replication fitness are shown (row 1; 95% CIs in parentheses) together with  $AIC_c$  values (row 2) and parameter estimates (rows 3–10), for each model fitted to the natural isolate dataset. Parameters that have separate values for the WT and MUT viruses are shown with the MUT estimate (e.g.  $\rho_{MUT}(0)$ ) below the WT estimate (e.g.  $\rho_{WT}(0)$ ).

Measure	Hypothesised model				
	$p$ -diff	$\beta$ -diff	$\tau_V$ -diff	$\tau_I$ -diff	$k$ -diff
RelFit	1.07 (1.02;2.59)	1.56 (1.05;2.92)	1.03 (1.01;1.10)	1.18 (1.06;1.39)	0.07 (0.05;6.06)
$AIC_c$	–719	–713	–717	–732	–728
$\log_{10}(V_{comb}^{TCD}(0))$	4.70 (–5.54; 4.70)	4.70 (–6.00; 4.70)	4.70 (–6.00; 4.70)	4.70 (–6.00; 4.70)	4.70 (–0.92; 4.70)
$\log_{10}(\rho(0))$	2.66(2.46; 2.85) 2.13(1.83; 2.39)	2.66(2.44; 2.86) 2.14(1.82; 2.41)	2.66(2.47; 2.84) 2.14(1.86; 2.37)	2.66(2.45; 2.86) 2.13(1.83; 2.41)	2.66(2.45; 2.86) 2.14(1.83; 2.41)
$\log_{10}(\beta)$	–5.62(–5.80; –1.00)	–4.00(–5.41; –1.04) –3.80(–5.36; –1.00)	–5.62(–5.74; –1.00)	–1.03(–4.50; –1.00)	–1.03(–3.53; –1.00)
$\log_{10}(k)$	1.38(0.22; 1.38)	1.38(0.16; 1.38)	1.38(0.19; 1.38)	1.38(0.14; 1.38)	1.38(0.29; 1.38) 0.23(0.05; 1.38)
$\log_{10}(\delta)$	0.90(–0.61; 0.90)	–0.52(–0.62; 0.90)	0.90(–0.60; 0.90)	–0.47(–0.56; –0.33) –0.54(–0.62; –0.43)	–0.49(–0.61; –0.40)
$\log_{10}(p)$	–0.46(–2.49; –0.25) –0.43(–2.29; –0.22)	(–2.50; –0.58)	–0.45(–2.35; –0.35)	–1.86(–2.40; –1.30)	–1.90(–2.41; –1.35)
$\log_{10}(c_h)$	0.21(0.05; 0.46)	0.20(0.02; 0.48)	0.31(0.07; 0.56) 0.27(–0.01; 0.53)	0.18(0.01; 0.32)	0.21(0.06; 0.35)
$\log_{10}(\xi)$	3.81(2.88; 4.54)	3.69(2.68; 4.62)	3.94(2.76; 4.54)	3.63(2.69; 4.53)	3.76(2.88; 4.61)



### 7.5. The H275Y mutation does not compromise the within-host replication fitness of the New17 OR virus, regardless of the hypothesised cause of fitness difference

Under each of the  $p$ -,  $\beta$ -,  $\tau_V$ -, and  $\tau_I$ -diff hypotheses, estimates of relative within-host fitness (Table 3) indicate that the New17 OR virus has significantly greater within-host fitness than the New163 OS virus, although in each case the lower bound of the 95% CI is close to one (equivalent fitness). Under the  $k$ -diff hypothesis, although the model fits the data relatively well (comparable  $AIC_c$ ), large uncertainty in the relative fitness estimate leads to a lack of evidence for a fitness difference. These results suggest that the H275Y mutation does not compromise the within-host replication fitness of the New17 OR virus; indeed the New17 OR virus likely has enhanced replication fitness compared with related OS strains.

## 8. The effects of the V241I and N369K neuraminidase mutations upon the replication fitness of H275Y OR strains

As discussed in Section 2, Butler et al. (2014) analysed reverse genetics (rg)-derived virus pairs in four additional competitive-mixtures experiments (see Table 1, rows 2–5) to investigate the effect of the V241I and N369K mutations upon the intrinsic fitness of H275Y OR strains.

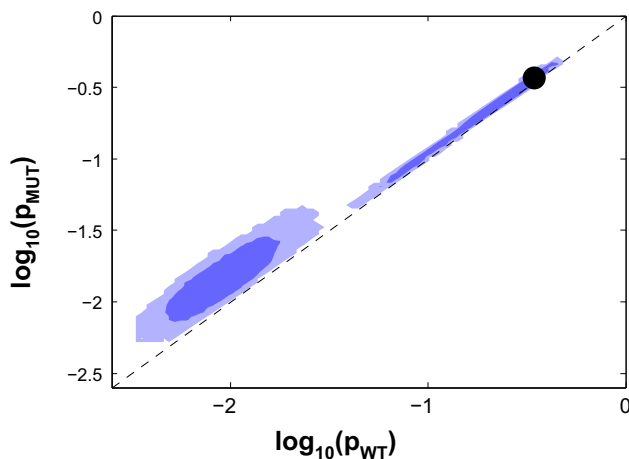


**Fig. 3.** Correlation between strain-dependent parameters. The best-fit (black dot) and 2-dimensional projections of the 68% LCR (dark blue contour) and 95% LCR (light blue contour) are shown for the two strain-dependent parameters in the  $p$ -diff model, when fitted to the natural isolate dataset. The dashed line shows the line of equivalent fitness. The estimated relative fitness ( $p_{MUT}/p_{WT}$ ) lies above the line (see Table 3). (For interpretation of the references to color in this figure caption, the reader is referred to the web version of this paper.)

**Table 5**

Relative replication fitness and  $AIC_c$  for the reverse genetics experiments. Best-fit estimates of relative within-host replication fitness are shown (95% CIs in parentheses) together with  $AIC_c$  values, for each model fitted to each of the reverse genetics experiments.

Dataset		Hypothesised model				
		$p$ -diff	$\beta$ -diff	$\tau_V$ -diff	$\tau_I$ -diff	$k$ -diff
rgNew17 OR vs.	RelFit	3.96 (1.17;6.83)	3.98 (1.12;7.02)	1.79 (1.10;4.58)	–	1.51 (1.08;7.39)
rgNew17I241VOR	$AIC_c$	–566	–562	–556	–529	–561
rgNew17 OR vs.	RelFit	3.14 (1.17;5.30)	2.44 (1.14;4.79)	2.05 (1.12;3.63)	1.35 (1.15;1.67)	1.94 (1.07;6.91)
rgNew17 K369N OR	$AIC_c$	–671	–659	–654	–650	–662
rgNew17 OR vs.	RelFit	1.82 (1.35;7.46)	6.33 (1.38;30.92)	1.38 (1.17;2.60)	1.49 (1.28;1.97)	2.97 (1.22;12.77)
rgNew17 K369N,I241V OR	$AIC_c$	–710	–719	–689	–708	–718
rgPerth261 N369K,V241I OR vs.	RelFit	1.86 (1.37;7.24)	5.43 (1.39;15.35)	1.71 (1.23;5.61)	1.31 (1.24;2.18)	1.74 (1.14;9.89)
rgPerth261 OR	$AIC_c$	–769	–776	–693	–690	–775

### 8.1. Fits to data

When fitting each alternative model to the rgNew17 OR vs. rgNew17 I241V OR (Figs. S6–S10), rgNew17 OR vs. rgNew17 K369N OR (Figs. S11–S15), rgNew17 OR vs. rgNew17 I241V, K369N OR (Figs. S16–S20), and rgPerth261 V241I, N369K OR vs. rgPerth261 OR (Figs. S21–S25) experiments, fits of infectious viral load, total viral load, and  $\rho(0)$  inoculum measurements are reproduced similarly well for all five hypothesised models (Figs. S6–S25, left and right columns). For a given hypothesised model, total vRNA A:B ratio dynamics are generally similar for all four reverse genetics experiments (Figs. S6–S25, centre column, solid blue lines) and also for the natural isolate experiment (Figs. 2 and S2–S5, centre column, solid blue lines). A notable exception to this consistency is evident in fits of the  $\tau_I$ -diff model, where the increase in total A:B ratio begins at different times for different experiments. This increase occurs latest when fitting the rgNew17 OR vs. rgNew17 I241V OR dataset (Fig. S9), such that the fitted total A:B ratio is substantially lower than pyrosequencing data in each of the mixed-infection ferrets during  $t \leq 4$  d(p.i.). This strong systematic failure indicates that the  $\tau_I$ -diff model produces a biologically implausible fit to the rgNew17 OR vs. rgNew17 I241V OR dataset. We do not interpret relative fitness estimates obtained from that particular experiment–model combination.

### 8.2. Differences in the ability of the five hypothesised models to reproduce observed infection dynamics

Table 5 also shows the  $AIC_c$  values for the five alternative hypothesised models fitted to each of the four reverse genetics experiments. For all four reverse genetics experiments the  $p$ -,  $\beta$ -, and  $k$ -diff models reproduce infection dynamics most accurately (lowest  $AIC_c$  values of the five models; note that  $AIC_c$  values are only compared within an experiment (row)). The  $\tau_V$ - and  $\tau_I$ -diff models produce relatively poor fits to data. Table 4, rows 2–5, provide a qualitative comparison of model performance when fitting the reverse genetics datasets. The varying ability of each model to reproduce infection dynamics across the different experiments is discussed further in Section 9.

### 8.3. The V241I and N369K substitutions improve the in vivo replication fitness of H1N1pdm09 H275Y OR viruses, regardless of the hypothesised cause of fitness difference

Table 5 shows estimates of relative within-host replication fitness for each of the five different hypothesised models fitted to the four rg experiments. For each of the three experiments that involve the rgNew17 OR virus, removing either one or both of the V241I and N369K substitutions results in a statistically significant reduction in within-host replication fitness. Conversely, adding the two substitutions to an early H1N1pdm09 virus improves its

within-host replication fitness. These results are consistent regardless of the hypothesised biological cause of fitness difference. These relative fitness estimates suggest that the V241I and N369K mutations improve the *in vivo* replication fitness of H1N1pdm09 H275Y OR viruses.

## 9. Discussion

Results from four of the five hypothesised models indicated that the New17 OR virus has significantly improved replication fitness relative to the New163 OS virus, while there was no evidence for a fitness difference under the *k*-diff hypothesis. If the New17 OR and New163 OS isolates are representative of other viruses from the HNE outbreak, then these results suggest that the H275Y mutation did not compromise the within-host fitness of HNE OR viruses. We come to this conclusion regardless of the hypothesised cause of fitness difference, reinforcing the conclusion presented in our earlier study (Butler et al., 2014) in which we used the *p*-diff hypothesis.

Our modelling analyses of the *rg* experiments demonstrates that the V241I and N369K mutations significantly increase the *in vivo* replication fitness of H1N1pdm09 H275Y OR strains. As the V241I and N369K mutations were present in the HNE viruses, this ability to compensate for the fitness cost of the H275Y mutation may have played an important role in enabling those OR viruses to spread amongst the community of the HNE region.

Pinilla et al. (2012) previously quantified relative fitness *in vitro* by allowing many model parameters to be strain-dependent and directly comparing estimates obtained for each strain. That same technique would not have been suitable for our purposes, as the *in vivo* experiments analysed here involved relatively sparse data and a more complex infection system compared with the *in vitro* experiments analysed by Pinilla et al. Instead, we investigated several different hypothesised causes of fitness differences separately, each involving a model with a single strain-dependent biological parameter. The fitting method employed here, while unable to identify some parameters (e.g.  $V^{TCID}(0)$  and *k*, which often have large uncertainties; Figs. S1 and S26–S49), was able to consistently generate precise estimates of relative fitness. These robust estimates were possible, despite a large degree of uncertainty and overlap in the strain-dependent parameter estimates, because each parameter pair was found to be highly correlated such that their ratio was well-estimated (e.g. Fig. 3), providing a viable method for quantifying relative fitness in competitive-mixtures experiments. These ratios involve comparatively little uncertainty primarily because each model is fitted to pyrosequencing data which, from the inoculum to the end of infection, show one strain consistently outgrowing the other across the different mixed-infection groups (Figs. 2 and S2–S25, centre column). Such consistent outgrowth in an experiment can only be reproduced if one strain-dependent parameter is larger than the other; hence their ratio is well-estimated regardless of uncertainty in the actual estimates of each parameter. Fitting this strong trend of outgrowth also tends to generate a consistent picture of which virus is fitter in a given experiment, regardless of the hypothesised biological cause of strain difference.

In the mixed-infection groups, each inoculum was prepared at the desired mixture (i.e. 20:80, 50:50, or 80:20) by measuring the infectivity titre of each virus, and then combining an appropriate amount of each virus together to generate the required proportion (Butler et al., 2014). However, for the natural isolate experiment, pyrosequencing measurements of the inocula were systematically lower than the intended proportions (Fig. 2). This systematic variation was also present (with a maximum discrepancy of almost 40%) in the *rgNew17 OR* vs. *rgNew17 K369N OR* (Fig. S11) and

*rgPerth261 V241I, N369K OR* vs. *rgPerth261 OR* (Fig. S21) experiments. Additionally, measurements of the rRT-PCR:TCID<sub>50</sub> ratio in the inocula varied systematically across the five different infection groups in each of these three experiments, suggesting that the two competing strains in each experiment had different ratios of infectious and total virus. Under the assumption that the initial *total vRNA:infectious virus* ratio ( $\rho(0)$ ) is strain-dependent, the co-infection model is capable of generating not only the systematic variation in rRT-PCR:TCID<sub>50</sub> ratio but also the systematic discrepancy between intended and measured inoculum proportions. Estimates of  $\rho(0)$  were consistent with observed trends in inocula data, in that  $\rho(0)$  was significantly different between strains in each of the three experiments where systematic variations were present, whereas no evidence of a significant difference was found in the other two experiments (data not shown). These results reinforce the importance of considering both infectious and total virus when analysing data from competitive-mixtures experiments.

Another possible explanation for the systematic discrepancy between intended and measured inoculum proportions is that the infectivity titres of each virus, taken prior to mixing, were simply inaccurate (e.g. if an A virus infectivity titre measurement had been inaccurate by just 0.1 : TCID<sub>50</sub>/ml, then an intended inoculum ratio of 50:50 would actually have led to a 56:44 ratio). This would lead to inoculum proportions that systematically differ from the intended proportions, however it would not explain the systematic change in rRT-PCR:TCID<sub>50</sub> ratio across different infection groups. Such a hypothesis is not as well supported by the data as the aforementioned hypothesis involving strain-dependence in  $\rho(0)$ . Nevertheless in future competitive-mixtures experiments it may be useful to more accurately measure the infectious concentration of each virus prior to mixing, e.g. by taking a greater number of replicates of infectivity measurements of each virus in order to reduce uncertainty ( $\approx 3$ –5 measurements were performed in the experiments analysed in this work). Such a reduction in uncertainty would allow further scrutiny of the plausibility of the assumption that the initial infectious proportion in each ferret is identical to the intended proportion in the corresponding inoculum.

Previous ferret competitive-mixtures experiments performed by Pinilla et al. (2012) indicated that an early H1N1pdm09 H275Y OR virus, in which the V241I and N369K mutations were absent, had reduced *in vivo* replication fitness relative to a related OS virus (each of these viruses were generated from the A/Québec/144147/09 isolate using reverse genetics techniques). Our results from the natural isolate competitive-mixtures experiment generally indicated an *in vivo* replication fitness advantage for the OR isolate from the HNE outbreak. If the isolates analysed in Pinilla et al. (2012) and here are representative of similar contemporaneously circulating viruses, then these contrasting results suggest an improvement in the fitness of late H1N1pdm09 OR viruses relative to early H1N1pdm09 OR viruses. This is consistent with the hypothesis that the V241I and N369K mutations enhance the fitness of H1N1pdm09 OR strains.

The *p*-,  $\beta$ -, and *k*-diff hypotheses (in which the infectious virus production rate, infectivity/mixing rate, and latent phase duration differ by strain, respectively) are supported not only by experimental results (Section 6) but also by results from previous *in vitro* modelling studies that compared the infection kinetics of H275Y MUT and related WT strains (Holder et al., 2011; Pinilla et al., 2012). Pinilla et al. (2012) found that the production rate of total vRNA from infected cells was statistically significantly different between WT and MUT strains in the H1N1pdm09 background, and that the average duration of the latent phase differed between WT and MUT strains in both the seasonal H1N1 and H1N1pdm09 backgrounds. The infecting time was also found to be different

between strains in the seasonal H1N1 background, consistent with the results of Holder et al. (2011) who performed a different analysis on the same dataset. Note that the infecting time ( $\tau_{\text{infect}} = \sqrt{2/[p\beta T(0)]}$ ) is dependent upon both  $p$  and  $\beta$  in the co-infection model; thus one or both of the equivalent parameters within the model used by Pinilla et al. may have been strain-dependent. The standard deviation in the distribution of latent phase durations ( $\sigma_L$ ) was also found by both Pinilla et al. (2012) and Holder et al. (2011) to be strain-dependent within the seasonal H1N1 background. Although we did not explicitly estimate  $\sigma_L$ , the estimates by Pinilla et al. (2012) and Holder et al. (2011) were roughly correlated with average latent phase duration ( $\tau_L$ ) in both the H1N1pdm09 (Pinilla et al., 2012) and seasonal H1N1 (Holder et al., 2011; Pinilla et al., 2012) backgrounds – the longer the average latent phase, the larger the standard deviation. This behaviour was replicated within the co-infection model, as splitting the  $L$  compartment into  $n_L$  stages generates an Erlang distribution for latent phase lifetimes with a standard deviation dependent upon the average latent phase duration via  $\sigma_L = \tau_L/\sqrt{n_L}$ .

For the natural isolate experiment, the  $k$ -diff model (i.e. latent phase duration differs by strain) and  $\tau_I$ -diff model (i.e. productive phase duration differs by strain) provided the best fits to data (Figs. S4 and S5, and Table 4). For the rg experiments, relatively poor fits were obtained when fitting the  $\tau_V$ -diff (viral clearance differs by strain) and  $\tau_I$ -diff models to the rgPerth261 V241I, N369K OR vs. rgPerth261 OR dataset, the  $\tau_V$ -diff model to the rgNew17 OR vs. rgNew17 I241V, K369N OR dataset, and the  $\tau_I$ -diff model to both the rgNew17 OR vs. rgNew17 I241V OR and rgNew17 OR vs. rgNew17 K369N OR datasets (Tables 4 and 5). It is interesting that the  $\tau_I$ -diff model produced the best fit to the natural isolate experiment, yet repeatedly produced poor fits to the rg experiments. Indeed biological differences between strains in the natural isolate experiment may be distinct from those in the rg experiments, as all virus pairs used in the rg experiments differ only via NA substitutions, whereas the viruses used in the natural isolate experiment differ via substitutions in both the NA gene and other genes. We have previously noted that none of the extra amino acid differences between the natural isolates have been linked to any functional process (Butler et al., 2014). Nonetheless it is possible that one or more of those substitutions have some yet to be established functional effect. This analysis highlights the potential to examine which hypothesised causes of fitness differences are the most plausible given observed competitive-mixtures data. Yet it is crucial to caution against overinterpretation of our results, as the co-infection model (1) involves relatively simple dynamics when compared with the complexities of the influenza infection system (Beauchemin and Handel, 2011; Smith and Perelson, 2011; Dobrovolny et al., 2013); and (2) is fitted to data that give only partial insight into those complex dynamics. More realistic within-host models coupled with more comprehensive datasets will be required to improve confidence in model selection.

Previous *in vitro* modelling of H275Y OR and related OS strains in the H1N1pdm09 background indicated that the ratio of total vRNA:infectious virus produced by infected cells significantly differed by strain (Pinilla et al., 2012). A hypothesis in which the ratio of total vRNA:infectious virus produced by infected cells ( $\xi$ ) is assumed to differ by strain could potentially generate strain-dependent viral load dynamics without an associated fitness difference, because only non-infectious virus production would differ by strain. We did not investigate such a model in this work because, in each competitive-mixtures experiment, observed outgrowth in pyrosequencing data across serial host-to-host transmission lines suggested that the fitness of each virus pair was indeed different (Butler et al., 2014). For future competitive-mixtures studies in which outgrowth is not evident in mixture

data, or in which multiple different hypotheses regarding functional differences between strains are investigated simultaneously, this alternative hypothesis may be a relevant biologically plausible scenario to investigate.

It is possible for predicted infectious A:B ratio dynamics to decouple from total vRNA ratio dynamics (e.g. Fig. S4, centre column). As infectious ratio dynamics provide more direct insight into relative fitness compared with total vRNA ratio dynamics, future development of an assay capable of measuring the infectious ratio would likely improve the capacity of competitive-mixtures experiments to assess relative fitness.

Furthermore, predicted infectious ratio dynamics sometimes differ substantially between different hypothesised models (e.g. compare the dashed black lines in the centre column of Fig. S2 to those of Fig. S4). These markedly different infectious ratios could lead to very different predictions regarding the proportion of each strain that is transmitted during any given transmission event. Such model-dependent behaviour can be explored in greater detail if transmission dynamics are incorporated into the co-infection model, and such an extended model is currently under development.

We have detailed a method for quantifying the relative within-host replication fitness of two competing influenza strains in competitive-mixtures experiments. Our results have relevance for drug-resistant influenza surveillance, and were consistent regardless of which underlying mechanism was assumed to generate a fitness difference between strains. The method may also have relevance for acute infections other than influenza, particularly those where drug-resistant or highly pathogenic strains have the potential to out-compete established strains.

## Acknowledgements

We thank Mathew Dafilis for his assistance with the implementation of an optimised ODE solver using the CVode package for MATLAB. We acknowledge the use of computing resources from the NeCTAR research cloud (<http://www.nectar.org.au>). NeCTAR is an Australian Government project conducted as part of the Super Science initiative and financed by the Education Investment Fund. This research was supported by a Victorian Life Sciences Computation Initiative (VLSCI) grant (VR0274) on its Peak Computing Facility at the University of Melbourne, an initiative of the Victorian Government, Australia. We also acknowledge the use of computing resources from the High Performance Computing Cluster at the University of Melbourne. The Melbourne WHO Collaborating Centre for Reference and Research on Influenza at the Peter Doherty Institute for Infection and Immunity is supported by the Australian Government Department of Health. Jodie McVernon was supported by a National Health and Medical Research Council Career Development Award (1061321). James McCaw was supported by an Australian Research Council Future Fellowship (110100250).

## Appendix A. Known functions of the NA surface protein

NA is important in facilitating the release of virus particles via cleavage of sialic acid residues, following the budding of those particles on the surface of infected cells (for related reviews, see Colman, 1994; Gubareva et al., 2000; Wagner et al., 2002; Nayak et al., 2004; Gong et al., 2007; Rossman and Lamb, 2011). Similarly, recent *in vitro* experiments have indicated that NA is capable of counteracting the effects of the antiviral factor tetherin, which also facilitates the release of progeny virions (Yondola et al., 2011). Other recent work has indicated that NA may be important in the budding of viral particles on the surface of infected cells and in the resulting morphogenesis of those particles (Lai et al., 2010;



Ushirogawa and Ohuchi, 2011; Yondola et al., 2011), and that the presence of NA alone within cells can lead to the release of non-infectious viral particles (Lai et al., 2010). Taken together, these known functions of NA indicate that it is important in the process of virion production, and in regulating the balance between the production of infectious and non-infectious virions.

Previous results have indicated that NA may be important in reducing the inhibiting effects of decoy receptors in mucins (Gubareva et al., 2000; Matrosovich et al., 2004; de Vries et al., 2012; Gerlach et al., 2012; Nishikawa et al., 2012; Wong et al., 2012), thus counteracting the effect of mucins in restricting the spatial spread of free virions throughout the site of infection. This function of NA may also inhibit host-driven clearance of virions from the site of infection, as decoy receptors in mucins, upon binding to free virions, also promote the clearance of those virions (Hatstrup and Gendler, 2008; Thornton et al., 2008).

Some studies have indicated that NA is important for influenza virus entry into susceptible cells (Suzuki et al., 2005; Su et al., 2009; Zhu et al., 2012). NA may also be important in determining the lifetime of infected cells (Morris et al., 1999; Gaur et al., 2012).

The results of Huang et al. (2008) suggest that NA also plays a role in inhibiting super-infection (i.e. the infection of a host cell by multiple influenza virions). However, we do not investigate strain-dependence in this process as a possible biological hypothesis for the source of fitness difference in this work, because a core assumption of the co-infection model was that susceptible cells are infected by a single infectious virion.

## Appendix B. Supplementary data

Supplementary data associated with this article can be found in the online version at <http://dx.doi.org/10.1016/j.jtbi.2015.07.003>

## References

- Arndt, U., Wennemuth, G., Barth, P., Nain, M., Al-Abed, Y., Meinhardt, A., Gerns, D., Bacher, M., 2002. Release of macrophage migration inhibitory factor and CXCL8/interleukin-8 from lung epithelial cells rendered necrotic by influenza A virus infection. *J. Virol.* 76 (18), 9298. <http://dx.doi.org/10.1128/JVI.76.18.9298>, URL: <http://jvi.asm.org/cgi/content/abstract/76/18/9298>.
- Baccam, P., Beauchemin, C.A.A., Macken, C.A., Hayden, F.G., Perelson, A.S., 2006. Kinetics of influenza A virus infection in humans. *J. Virol.* 80 (15), 7590–7599. <http://dx.doi.org/10.1128/JVI.01623-05>, URL: <http://www.ncbi.nlm.nih.gov/pubmed/16840338>.
- Beauchemin, C.A.A., Handel, A., 2011. A review of mathematical models of influenza A infections within a host or cell culture: lessons learned and challenges ahead. *BMC Pub. Health* 11 (Suppl 1), S7. <http://dx.doi.org/10.1186/1471-2458-11-S1-S7>, URL: <http://www.ncbi.nlm.nih.gov/pubmed/21356136>.
- Beauchemin, C.A.A., McSharry, J.J., Drusano, G.L., Nguyen, J.T., Went, G.T., Ribeiro, R. M., Perelson, A.S., 2008. Modeling amantadine treatment of influenza A virus in vitro. *J. Theor. Biol.* 254 (2), 439–451. <http://dx.doi.org/10.1016/j.jtbi.2008.05.031>, URL: <http://www.pubmedcentral.nih.gov/articlerender.fcgi?artid=2663526&tool=pmcentrez&rendertype=abstract>.
- Burnham, K.P., Anderson, D.R., 2004. Multimodel inference: understanding aic and bic in model selection. *Sociol. Methods Res.* 33 (2), 261–304. <http://dx.doi.org/10.1177/0049124104268644>, URL: <http://smr.sagepub.com/cgi/doi/10.1177/0049124104268644>.
- Butler, J., Hooper, K.A., Petrie, S., Lee, R., Maurer-Stroh, S., Reh, L., Guarnaccia, T., Baas, C., Xue, L., Vitesnik, S., Leang, S.-K., McVernon, J., Kelso, A., Barr, I.G., McCaw, J.M., Bloom, J.D., Hurt, A.C., 2014. Estimating the fitness advantage conferred by permissive neuraminidase mutations in recent oseltamivir-resistant A(H1N1)pdm09 influenza viruses. *PLoS Pathog.* 10 (4), e1004065. <http://dx.doi.org/10.1371/journal.ppat.1004065>, URL: <http://dx.plos.org/10.1371/journal.ppat.1004065>.
- Centers for Disease Control and Prevention (CDC), 2008. Update: Influenza activity –United States, September 30, 2007–April 5, 2008, and composition of the 2008–09 influenza vaccine. *MMWR Morb. Mortal. Wkly. Rep.* 57 (15) 404–409.
- Centers for Disease Control and Prevention (CDC), 2009. Update: influenza activity –United States, September 28, 2008–April 4, 2009, and composition of the 2009–10 influenza vaccine. *MMWR Morb. Mortal. Wkly. Rep.* 58 (14) 369–374. URL: <http://www.ncbi.nlm.nih.gov/pubmed/21918493>.
- Colman, P.M., 1994. Influenza virus neuraminidase: structure, antibodies, and inhibitors. *Protein Sci.* 3 (10), 1687–1696. <http://dx.doi.org/10.1002/pro.5560031007>, URL: <http://www.pubmedcentral.nih.gov/articlerender.fcgi?artid=2142611&tool=pmcentrez&rendertype=abstract>.
- de Vries, E., de Vries, R.P., Wienholts, M.J., Floris, C.E., Jacobs, M.-S., van den Heuvel, A., Rottier, P.J.M., de Haan, C.A.M., 2012. Influenza A virus entry into cells lacking sialylated N-glycans. *Proc. Natl. Acad. Sci. U.S.A.* 109 (19), 7457–7462. <http://dx.doi.org/10.1073/pnas.1200987109>, URL: <http://www.pubmedcentral.nih.gov/articlerender.fcgi?artid=3358892&tool=pmcentrez&rendertype=abstract>.
- Dharan, N.J., Gubareva, L.V., Meyer, J.J., Okomo-Adhiambo, M., McClinton, R.C., Marshall, S.A., George St, K., Epperson, S., Brammer, L., Klimov, A.I., Bresee, J.S., Fry, A.M., 2009. Infections with oseltamivir-resistant influenza A(H1N1) virus in the United States. *J. Am. Med. Assoc.* 301 (10), 1034–1041. <http://dx.doi.org/10.1001/jama.2009.294>, URL: <http://www.ncbi.nlm.nih.gov/pubmed/21737049>.
- Dobrovolsky, H.M., Reddy, M.B., Kamal, M.A., Rayner, C.R., Beauchemin, C.A.A., 2013. Assessing mathematical models of influenza infections using features of the immune response. *PLoS ONE* 8 (2), e57088. <http://dx.doi.org/10.1371/journal.pone.0057088>.
- Donaldson, J., Schnabel, R., 1987. Computational experience with confidence regions and confidence intervals for nonlinear least squares. *Technometrics* 29 (1), 67–82. URL: <http://www.jstor.org/stable/10.2307/1269884>.
- Gaur, P., Ranjan, P., Sharma, S., Patel, J.R., Bowzard, J.B., Rahman, S.K., Kumari, R., Gangappa, S., Katz, J.M., Cox, N.J., Lal, R.B., Sambhara, S., Lal, S.K., 2012. Influenza A virus neuraminidase protein enhances cell survival through interaction with carcinoembryonic antigen-related cell adhesion molecule 6 (CEACAM6) protein. *J. Biol. Chem.* 287 (18), 15109–15117. <http://dx.doi.org/10.1074/jbc.M111.328070>, URL: <http://www.pubmedcentral.nih.gov/articlerender.fcgi?artid=3340274&tool=pmcentrez&rendertype=abstract>.
- Gaush, C.R., Smith, T.F., 1968. Replication and plaque assay of influenza virus in an established line of canine kidney cells. *Appl. Microbiol.* 16 (4), 588–594. URL: <http://www.pubmedcentral.nih.gov/articlerender.fcgi?artid=547475&tool=pmcentrez&rendertype=abstract>.
- Gerlach, T., Kühling, L., Uhlenhorff, J., Laukemper, V., Matrosovich, T., Czudai-Matwich, V., Schwalm, F., Klenk, H.-D., Matrosovich, M., 2012. Characterization of the neuraminidase of the H1N1/09 pandemic influenza virus. *Vaccine* 30 (51), 7348–7352. <http://dx.doi.org/10.1016/j.vaccine.2012.09.078>, URL: <http://www.ncbi.nlm.nih.gov/pubmed/23063828>.
- Gong, J., Xu, W., Zhang, J., 2007. Structure and functions of influenza virus neuraminidase. *Curr. Med. Chem.* 14 (1), 113–122. URL: <http://www.ncbi.nlm.nih.gov/pubmed/17266572>.
- Grienke, U., Schmidtke, M., von Grafenstein, S., Kirchmair, J., Liedl, K.R., Röllinger, J. M., 2012. Influenza neuraminidase: a druggable target for natural products. *Nat. Prod. Rep.* 29 (1), 11–36. <http://dx.doi.org/10.1039/c1np00053e>, URL: <http://www.ncbi.nlm.nih.gov/pubmed/22025274>.
- Gubareva, L.V., Kaiser, L., Hayden, F.G., 2000. Influenza virus neuraminidase inhibitors. *The Lancet* 355, 827–835. URL: <http://www.sciencedirect.com/science/article/pii/S0140673699114338>.
- Handel, A., Longini, I.M., Antia, R., 2007. Neuraminidase inhibitor resistance in influenza: assessing the danger of its generation and spread. *PLoS Comput. Biol.* 3 (12), e240. <http://dx.doi.org/10.1371/journal.pcbi.0030240>, URL: <http://www.pubmedcentral.nih.gov/articlerender.fcgi?artid=2134965&tool=pmcentrez&rendertype=abstract>.
- Hatstrup, C.L., Gendler, S.J., 2008. Structure and function of the cell surface (tethered) mucins. *Annu. Rev. Physiol.* 70, 431–457. <http://dx.doi.org/10.1146/annurev.physiol.70.113006.100659>, URL: <http://www.ncbi.nlm.nih.gov/pubmed/17850209>.
- Hauge, S.H., Dudman, S., Borgen, K., Lackenby, A., Hungnes, O., 2009. Oseltamivir-resistant influenza viruses A (H1N1), Norway, 2007–08. *Emerg. Infect. Dis.* 15 (2), 155–162. <http://dx.doi.org/10.3201/eid1502.081031>, URL: <http://www.cdc.gov/eid/content/15/2/155.htm>.
- Holder, B.P., Beauchemin, C.A.A., 2011. Exploring the effect of biological delays in kinetic models of influenza within a host or cell culture. *BMC Pub. Health* 11 (Suppl 1), S10. <http://dx.doi.org/10.1186/1471-2458-11-S1-S10>, URL: <http://www.ncbi.nlm.nih.gov/pubmed/21356129>.
- Holder, B.P., Simon, P., Liao, L.E., Abed, Y., Bouhy, X., Beauchemin, C.A.A., Boivin, G., 2011. Assessing the in vitro fitness of an oseltamivir-resistant seasonal A/H1N1 influenza strain using a mathematical model. *PLoS ONE* 6 (3), e14767. <http://dx.doi.org/10.1371/journal.pone.0014767>, URL: <http://www.pubmedcentral.nih.gov/articlerender.fcgi?artid=3063785&tool=pmcentrez&rendertype=abstract>.
- Horsfall, F.L., 1954. On the reproduction of influenza virus. Quantitative studies with procedures which enumerate infective and hemagglutinating virus particles. *J. Exp. Med.* 100 (2), 135–161. URL: <http://www.ncbi.nlm.nih.gov/pmc/articles/PMC2136364>.
- Huang, I.-C., Li, W., Sui, J., Marasco, W., Choe, H., Farzan, M., 2008. Influenza A virus neuraminidase limits viral superinfection. *J. Virol.* 82 (10), 4834–4843. <http://dx.doi.org/10.1128/JVI.00079-08>, URL: <http://www.pubmedcentral.nih.gov/articlerender.fcgi?artid=2346733&tool=pmcentrez&rendertype=abstract>.
- Hurt, A.C., Ernest, J., Deng, Y.-M., Iannello, P., Besselaar, T.G., Birch, C., Buchy, P., Chittaganpitch, M., Chiu, S.-C., Dwyer, D., Guigon, A., Harrower, B., Kei, I.P., Kok, T., Lin, C., McPhie, K., Mohd, A., Olveda, R., Panayotou, T., Rawlinson, W., Scott, L., Smith, D., D'Souza, H., Komadina, N., Shaw, R., Kelso, A., Barr, I.G., 2009. Emergence and spread of oseltamivir-resistant A(H1N1) influenza viruses in Oceania South East Asia and South Africa. *Antivir. Res.* 83 (1), 90–93. <http://dx.doi.org/10.1016/j.antiviral.2009.03.003> <http://www.ncbi.nlm.nih.gov/pubmed/19501261>.
- Hurt, A.C., Nor'e, S.S., McCaw, J.M., Fryer, H.R., Mosse, J., McLean, A.R., Barr, I.G., 2010. Assessing the viral fitness of oseltamivir-resistant influenza viruses in



- ferrets, using a competitive-mixtures model. *J. Virol.* 84 (18), 9427–9438. <http://dx.doi.org/10.1128/JVI.00373-10>, URL: <http://www.pubmedcentral.nih.gov/articlerender.fcgi?artid=2937593&tool=pmcentrez&rendertype=abstract>.
- Kelso, A., Hurt, A.C., 2012. Drug-resistant influenza viruses: why fitness matters. *Nat. Med.* 18 (10), 1470–1472.
- Lai, J.C.C., Chan, W.W.L., Kien, F., Nicholls, J.M., Peiris, J.S.M., Garcia, J.-M., 2010. Formation of virus-like particles from human cell lines exclusively expressing influenza neuraminidase. *J. Gen. Virol.* 91 (Pt 9), 2322–2330. <http://dx.doi.org/10.1099/vir.0.019935-0>, URL: <http://www.ncbi.nlm.nih.gov/pubmed/20505010>.
- Möhler, L., Flockerzi, D., Sann, H., Reichl, U., 2005. Mathematical model of influenza A virus production in large-scale microcarrier culture. *Biotechnol. Bioeng.* 90 (1), 46–58. <http://dx.doi.org/10.1002/bit.20363> <http://www.ncbi.nlm.nih.gov/pubmed/15736163>.
- Marée, A.F.M., Keulen, W., Boucher, C.A.B., de Boer, R.J., 2000. Estimating relative fitness in viral competition experiments. *J. Virol.* 74 (23), 11067–11072, URL: <http://www.pubmedcentral.nih.gov/articlerender.fcgi?artid=113186&tool=pmcentrez&rendertype=abstract>.
- Matrosovich, M.N., Matrosovich, T.Y., Gray, T., Roberts, N.A., Klenk, H.-D., 2004. Neuraminidase is important for the initiation of influenza virus infection in human airway epithelium. *J. Virol.* 78 (22), 12665–12667. <http://dx.doi.org/10.1128/JVI.78.22.12665>.
- Meijer, A., Lackenby, A., Hungnes, O., Lina, B., van der Werf, S., Schweiger, B., Opp, M., Paget, J., van der Kasstele, J., Hay, A., Zambon, M., 2009. Oseltamivir-resistant influenza virus A (H1N1), Europe, 2007–08 season. *Emerg. Infect. Dis.* 15 (4), 552–560. <http://dx.doi.org/10.3201/eid1504.081280>, URL: <http://www.cdc.gov/eid/content/15/4/552.htm>.
- Miao, H., Hollenbaugh, J.A., Zand, M.S., Holden-Wiltse, J., Mosmann, T.R., Perelson, A.S., Wu, H., Topham, D.J., 2010. Quantifying the early immune response and adaptive immune response kinetics in mice infected with influenza A virus. *J. Virol.* 84 (13), 6687–6698. <http://dx.doi.org/10.1128/JVI.00266-10>, URL: <http://www.pubmedcentral.nih.gov/articlerender.fcgi?artid=2903284&tool=pmcentrez&rendertype=abstract>.
- Morris, S.J., Price, G.E., Barnett, J.M., Hiscox, S.A., Smith, H., Sweet, C., 1999. Role of neuraminidase in influenza virus-induced apoptosis. *J. Gen. Virol.* 80 (1), 137–146, URL: <http://vir.sgmjournals.org/content/80/1/137.short>.
- Moscona, A., 2009. Global transmission of oseltamivir-resistant influenza. *New Engl. J. Med.* 360 (10), 953–956. <http://dx.doi.org/10.1056/NEJMp0900648>, URL: <http://www.pubmedcentral.nih.gov/articlerender.fcgi?artid=3089626&tool=pmcentrez&rendertype=abstract>.
- Nayak, D.P., Hui, E.K.-W., Barman, S., 2004. Assembly and budding of influenza virus. *Virus Res.* 106 (2), 147–165. <http://dx.doi.org/10.1016/j.virusres.2004.08.012>, URL: <http://www.ncbi.nlm.nih.gov/pubmed/15567494>.
- Nicholson, K.G., Wood, J.M., Zambon, M., 2003. Influenza. *Lancet* 362 (9397), 1733–1745. [http://dx.doi.org/10.1016/S0140-6736\(03\)14854-4](http://dx.doi.org/10.1016/S0140-6736(03)14854-4), URL: <http://www.ncbi.nlm.nih.gov/pubmed/19799843>.
- Nishikawa, T., Shimizu, K., Tanaka, T., Kuroda, K., Takayama, T., Yamamoto, T., Hanada, N., Hamada, Y., 2012. Bacterial neuraminidase rescues influenza virus replication from inhibition by a neuraminidase inhibitor. *PLoS ONE* 7 (9), e45371. <http://dx.doi.org/10.1371/journal.pone.0045371>, URL: <http://www.pubmedcentral.nih.gov/articlerender.fcgi?artid=3445474&tool=pmcentrez&rendertype=abstract>.
- Orthel, F.W., 1972. Influenza virus titrations and the inhibitor of hemagglutination in normal allantoic fluid. *Archiv für die gesamte Virusforschung* 38 (4), 347–356, URL: <http://www.ncbi.nlm.nih.gov/pubmed/5083408>.
- Paucker, K., Henle, W., 1955. Studies on host-virus interactions in the chick embryo-influenza virus system. XI. The effect of partial inactivation of standard seed virus at 37°C upon the progeny. *J. Exp. Med.* 101 (5), 479–492, URL: <http://jem.rupress.org/content/90/1/23.abstract>.
- Pawelek, K.A., Huynh, G.T., Quinlan, M., Cullinane, A., Rong, L., Perelson, A.S., 2012. Modeling within-host dynamics of influenza virus infection including immune responses. *PLoS Comput. Biol.* 8 (6), e1002588. <http://dx.doi.org/10.1371/journal.pcbi.1002588>, URL: <http://www.pubmedcentral.nih.gov/articlerender.fcgi?artid=3386161&tool=pmcentrez&rendertype=abstract>.
- Petrie, S.M., Guarnaccia, T., Laurie, K.L., Hurt, A.C., McVernon, J., McCaw, J.M., 2013. Reducing uncertainty in within-host parameter estimates of influenza infection by measuring both infectious and total viral load. *PLoS ONE* 8 (5), e64098. <http://dx.doi.org/10.1371/journal.pone.0064098>, URL: <http://www.pubmedcentral.nih.gov/articlerender.fcgi?artid=3655064&tool=pmcentrez&rendertype=abstract>.
- Pinilla, L.T., Holder, B.P., Abed, Y., Boivin, G., Beauchemin, C.A.A., 2012. The H275Y neuraminidase mutation of the pandemic A/H1N1 influenza virus lengthens the eclipse phase and reduces viral output of infected cells, potentially compromising fitness in ferrets. *J. Virol.* 86 (19), 10651–10660. <http://dx.doi.org/10.1128/JVI.07244-11>, URL: <http://www.ncbi.nlm.nih.gov/pubmed/22837199>.
- Rossman, J.S., Lamb, R.A., 2011. Influenza virus assembly and budding. *Virology* 411 (2), 229–236. <http://dx.doi.org/10.1016/j.virol.2010.12.003>, URL: <http://www.pubmedcentral.nih.gov/articlerender.fcgi?artid=3086653&tool=pmcentrez&rendertype=abstract>.
- Saenz, R.A., Quinlan, M., Elton, D., Macrae, S., Blunden, A.S., Mumford, J.A., Daly, J. M., Digard, P., Cullinane, A., Grenfell, B.T., McCauley, J.W., Wood, J.L.N., Gog, J.R., 2010. Dynamics of influenza virus infection and pathology. *J. Virol.* 84 (8), 3974–3983. <http://dx.doi.org/10.1128/JVI.02078-09>, URL: <http://www.ncbi.nlm.nih.gov/pubmed/20130053>.
- Schulze-Horsel, J., Schulze, M., Agalaridis, G., Genzel, Y., Reichl, U., 2009. Infection dynamics and virus-induced apoptosis in cell culture-based influenza vaccine production—flow cytometry and mathematical modeling. *Vaccine* 27 (20), 2712–2722. <http://dx.doi.org/10.1016/j.vaccine.2009.02.027>, URL: <http://www.ncbi.nlm.nih.gov/pubmed/19428884>.
- Schwaab, M., Bisciajari, E., Monteiro, J., Pinto, J., 2008. Nonlinear parameter estimation through particle swarm optimization. *Chem. Eng. Sci.* 63 (6), 1542–1552. <http://dx.doi.org/10.1016/j.ces.2007.11.024>, URL: <http://linkinghub.elsevier.com/retrieve/pii/S0009250907008755>.
- Sheu, T.G., Deyde, V.M., Okomo-Adhiambo, M., Garten, R.J., Xu, X., Bright, R.A., Butler, E.N., Wallis, T.R., Klimov, A.I., Gubareva, L.V., 2008. Surveillance for neuraminidase inhibitor resistance among human influenza A and B viruses circulating worldwide from 2004 to 2008. *Antimicrob. Agents Chemother.* 52 (9), 3284–3292. <http://dx.doi.org/10.1128/AAC.00555-08>, URL: <http://www.pubmedcentral.nih.gov/articlerender.fcgi?artid=2533500&tool=pmcentrez&rendertype=abstract>.
- Smith, A.M., Perelson, A.S., 2011. Influenza A virus infection kinetics: quantitative data and models. *Wiley Interdiscip. Rev.: Syst. Biol. Med.* 3 (4), 429–445. <http://dx.doi.org/10.1002/wsbm.129>, URL: <http://onlinelibrary.wiley.com/doi/10.1002/wsbm.129/abstract>.
- Smith, A.M., Adler, F.R., McAuley, J.L., Gutenkunst, R.N., Ribeiro, R.M., McCullers, J.A., Perelson, A.S., 2011. Effect of 1918 PB1-F2 expression on influenza A virus infection kinetics. *PLoS Comput. Biol.* 7 (2), e1001081. <http://dx.doi.org/10.1371/journal.pcbi.1001081>, URL: <http://dx.plos.org/10.1371/journal.pcbi.1001081>.
- Su, B., Wurtzer, S., Rameix-Welti, M.-A., Dwyer, D.E., van der Werf, S., Naffakh, N., Clavel, F., Labrosse, B., 2009. Enhancement of the influenza A hemagglutinin (HA)-mediated cell-cell fusion and virus entry by the viral neuraminidase (NA). *PLoS ONE* 4 (12), e8495. <http://dx.doi.org/10.1371/journal.pone.0008495>, URL: <http://www.ncbi.nlm.nih.gov/pubmed/20041119>.
- Sullivan, S.J., Jacobson, R.M., Dowdle, W.R., Poland, G.A., 2010. 2009 H1N1 influenza. *Mayo Clin. Proc.*, Mayo Clin. 85 (1), 64–76. <http://dx.doi.org/10.4065/mcp.2009.0588>, URL: <http://www.ncbi.nlm.nih.gov/pubmed/20007905>.
- Suzuki, T., Takahashi, T., Guo, C.-T., Hidari, K.I.-P.J., Miyamoto, D., Goto, H., Kawaoka, Y., Suzuki, Y., 2005. Sialidase activity of influenza A virus in an endocytic pathway enhances viral replication. *J. Virol.* 79 (18), 11705–11715. <http://dx.doi.org/10.1128/JVI.79.18.11705>, URL: <http://jvi.asm.org/content/79/18/11705.short>.
- Thornton, D.J., Rousseau, K., McGuckin, M.A., 2008. Structure and function of the polymeric mucins in airways mucus. *Annu. Rev. Physiol.* 70, 459–486. <http://dx.doi.org/10.1146/annurev.physiol.70.113006.100702>, URL: <http://www.ncbi.nlm.nih.gov/pubmed/17850213>.
- Ushirogawa, H., Ohuchi, M., 2011. Novel antiviral activity of neuraminidase inhibitors against an avian influenza A virus. *Virol. J.* 8, 411. <http://dx.doi.org/10.1186/1743-422X-8-411>, URL: <http://www.pubmedcentral.nih.gov/articlerender.fcgi?artid=3170304&tool=pmcentrez&rendertype=abstract>.
- Wagner, R., Matrosovich, M., Klenk, H.-D., 2002. Functional balance between haemagglutinin and neuraminidase in influenza virus infections. *Rev. Med. Virol.* 12 (3), 159–166. <http://dx.doi.org/10.1002/rmv.352>, URL: <http://www.ncbi.nlm.nih.gov/pubmed/11987141>.
- Wong, D.D.Y., Choy, K.-T., Chan, R.W.Y., Sia, S.F., Chiu, H.-P., Cheung, P.P.H., Chan, M. C.W., Peiris, J.S.M., Yen, H.-L., 2012. Comparable fitness and transmissibility between oseltamivir-resistant pandemic 2009 and seasonal H1N1 influenza viruses with the H275Y neuraminidase mutation. *J. Virol.* 86 (19), 10558–10570. <http://dx.doi.org/10.1128/JVI.00985-12>, URL: <http://www.ncbi.nlm.nih.gov/pubmed/22811535>.
- Wu, H., Huang, Y., Dykes, C., Liu, D., Ma, J., Perelson, A.S., Demeter, L.M., 2006. Modeling and estimation of replication fitness of human immunodeficiency virus type 1 in vitro experiments by using a growth competition assay. *J. Virol.* 80 (5), 2380–2389. <http://dx.doi.org/10.1128/JVI.80.5.2380>, URL: <http://jvi.asm.org/cgi/content/abstract/80/5/2380>.
- Yondola, M.A., Fernandes, F., Belicha-Villanueva, A., Uccellini, M., Gao, Q., Carter, C., Palese, P., 2011. Budding capability of the influenza virus neuraminidase can be modulated by tetherin. *J. Virol.* 85 (6), 2480–2491. <http://dx.doi.org/10.1128/JVI.02188-10>, URL: <http://www.pubmedcentral.nih.gov/articlerender.fcgi?artid=3067929&tool=pmcentrez&rendertype=abstract>.
- Zhirnov, O., Klenk, H.-D., 2003. Human influenza A viruses are proteolytically activated and do not induce apoptosis in CACO-2 cells. *Virology* 313 (1), 198–212. [http://dx.doi.org/10.1016/S0042-6822\(03\)00264-2](http://dx.doi.org/10.1016/S0042-6822(03)00264-2), URL: <http://linkinghub.elsevier.com/retrieve/pii/S0042682203002642>.
- Zhu, X., McBride, R., Nycholat, C.M., Yu, W., Paulson, J.C., Wilson, I.A., 2012. Influenza virus neuraminidases with reduced enzymatic activity that avidly bind sialic acid receptors. *J. Virol.* 86 (24), 13371–13383. <http://dx.doi.org/10.1128/JVI.01426-12>, URL: <http://www.ncbi.nlm.nih.gov/pubmed/23015718>.